Three-Dimensional Solution Structure of α-Conotoxin MII by NMR Spectroscopy: Effects of Solution Environment on Helicity † , ‡

ARTICLE *in* BIOCHEMISTRY · DECEMBER 1998

Impact Factor: 3.02 · DOI: 10.1021/bi981535w · Source: PubMed

6 AUTHORS, INCLUDING:

Jon-Paul Bingham
University of Hawai'i at Mānoa

44 PUBLICATIONS **495** CITATIONS

SEE PROFILE

Three-Dimensional Solution Structure of α-Conotoxin MII by NMR Spectroscopy: Effects of Solution Environment on Helicity[†,‡]

Justine M. Hill,[§] Clasien J. Oomen,[§,||] Les P. Miranda,[§] Jon-Paul Bingham,[⊥] Paul F. Alewood,[§] and David J. Craik*[,§]

Centre for Drug Design and Development and Department of Biochemistry, The University of Queensland, Brisbane, Queensland 4072, Australia

Received June 29, 1998

ABSTRACT: α-Conotoxin MII, a 16-residue polypeptide from the venom of the piscivorous cone snail *Conus magus*, is a potent and highly specific blocker of mammalian neuronal nicotinic acetylcholine receptors composed of α3β2 subunits. The role of this receptor type in the modulation of neurotransmitter release and its relevance to the problems of addiction and psychosis emphasize the importance of a structural understanding of the mode of interaction of MII with the α3β2 interface. Here we describe the three-dimensional solution structure of MII determined using 2D ^{1}H NMR spectroscopy. Structural restraints consisting of 376 interproton distances inferred from NOEs and 12 dihedral restraints derived from spin−spin coupling constants were used as input for simulated annealing calculations and energy minimization in the program X-PLOR. The final set of 20 structures is exceptionally well-defined with mean pairwise rms differences over the whole molecule of 0.07 Å for the backbone atoms and 0.34 Å for all heavy atoms. MII adopts a compact structure incorporating a central segment of α-helix and β-turns at the N- and C-termini. The molecule is stabilized by two disulfide bonds, which provide cross-links between the N-terminus and both the middle and C-terminus of the structure. The susceptibility of the structure to conformational change was examined using several different solvent conditions. While the global fold of MII remains the same, the structure is stabilized in a more hydrophobic environment provided by the addition of acetonitrile or trifluoroethanol to the aqueous solution. The distribution of amino acid side chains in MII creates distinct hydrophobic and polar patches on its surface that may be important for the specific interaction with the α3β2 neuronal nAChR. A comparison of the structure of MII with other neuronal-specific α-conotoxins provides insights into their mode of interaction with these receptors.

The venoms of *Conus* snails typically contain complex mixtures of small disulfide-rich peptides (conotoxins), each targeted to a particular ion channel or macromolecular receptor. Targets currently identified include voltage-sensitive sodium, calcium, and potassium channels and *N*-methyl-D-aspartyl-glutamate, vasopressin, and acetylcholine receptors. Many of these conotoxins have been applied by researchers as pharmacological tools and biochemical probes for investigating the structure and function of receptors critical to the functioning of the neuromuscular system (*1*). The high potency and specificity, and convenient chemical synthesis of conotoxins also make them attractive leads in drug design programs (*2*).

Of interest in this study are the α-conotoxins which target the nicotinic acetylcholine receptor (nAChR).[1] α-Conotoxins are widespread in the venoms of cone snails and have been isolated from piscivorous, molluscivorous, and vermivorous species (*3*−*12*). These toxins are valuable ligands for probing structure−function relationships of various nAChR subtypes as they are potent antagonists and exhibit marked selectivity between the peripheral and neuronal forms of the receptor. Typically, the α-conotoxins are 12−18 residues in length and are characterized by the presence of two conserved disulfide bonds (Figure 1). The I−III and II−IV connectivity of the four constituent cysteine residues produces a significantly more stable and well-defined structure than alternative arrangements of the disulfide bonds, as demonstrated recently in a study of the native and non-native disulfide isomers of α-conotoxin GI (*13*). However, the number of amino acids present between the cysteine residues varies, giving rise to the α3/5, α4/7, and α4/3 subclasses of α-conotoxins.

[†] This work was supported in part by the Australian Research Council (D.J.C.) and Australian Postgraduate Awards (J.M.H. and L.P.M.).

[‡] The NMR restraints and coordinates of the final structures have been deposited at the Brookhaven Protein Data Bank under the accession code 1MII.

* To whom correspondence should be addressed. Fax: +61-7-3365-2487. Phone: +61-7-3365-4945. E-mail: d.craik@mailbox.uq.edu.au.

[§] Centre for Drug Design and Development.

[||] Present address: Department of Biochemistry, Wageningen Agricultural University, Wageningen, The Netherlands.

[⊥] Department of Biochemistry.

[1] Abbreviations: nAChR, nicotinic acetylcholine receptor; MII, α-conotoxin MII; CD, circular dichroism; NMR, nuclear magnetic resonance; 2D, two dimensional; DQF-COSY, double-quantum-filtered 2D correlation spectroscopy; E-COSY, exclusive COSY; TOCSY, 2D total correlation spectroscopy; NOE, nuclear Overhauser effect; NOESY, 2D NOE spectroscopy; SA, simulated annealing; WATERGATE, water suppression by gradient-tailored excitation; rms, root mean square; TFE, 2,2,2-trifluoroethanol; Boc, *tert*-butoxycarbonyl; ESMS, electrospray ionization mass spectrometry; RP-HPLC, reversed-phase high performance liquid chromatography; DSS, 2,2-dimethyl-2-silapentane-5-sulfonate.

10.1021/bi981535w CCC: $15.00
Published on Web 10/23/1998

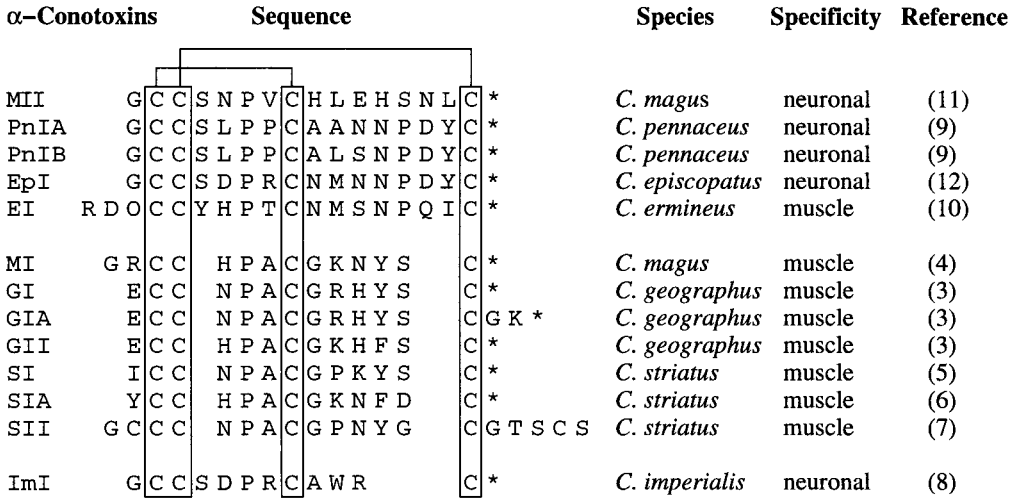

FIGURE 1: Amino acid sequences and conserved cysteine framework (boxed) of the α-conotoxins (* = amidated C-terminus, O = *trans*-4-hydroxyproline, and Y = sulfotyrosine). Toxins in the α4/7, α3/5, and α4/3 structural subclasses are shown in the upper, middle, and lower sections of the sequence alignment, respectively, and the nAChR specificity of each toxin is indicated. Note that SII has an additional disulfide bond, and the connectivities have not yet been determined.

The recently identified α-conotoxin MII from *Conus magus* belongs to the α4/7 subclass (Figure 1) and is a potent and highly specific blocker of mammalian neuronal nAChRs composed of α3β2 subunits. MII was first reported by Cartier et al. (*11*) following the electrophysiological screening of RP-HPLC fractions of duct venom against cloned nAChRs expressed in *Xenopus* oocytes. We have independently isolated and characterized MII as part of a comprehensive study of the milked venom of *C. magus*. It is notable that while MII is only present in small quantities in duct venom (*11*), it constitutes a major component of the milked venom profile (J.-P. Bingham, unpublished results).

The nAChRs are members of a gene superfamily of pentameric ligand-gated ion channels and are present in muscle and neuronal tissues. Neuronal nAChRs are much more diverse than those in muscle and are believed to be made up of combinations of α (α2−α7, α9) and β (β2−β4) subunits (*14*). Activation of distinct subtypes of these presynaptic nAChRs by nicotinic agonists can selectively regulate the release of different neurotransmitters including dopamine, norepinephrine, glutamate, and acetylcholine (*15*−*17*). Such receptors have also been implicated in the pathophysiology of several neuropsychiatric disorders including schizophrenia, Alzheimer's disease, Parkinson's disease, and Tourette's syndrome (*15*). Despite their importance, few of the nicotinic antagonists identified to date are highly selective between the multiple neuronal nAChR subtypes. Thus the ability of MII to target α3β2 neuronal nAChRs with high specificity has considerable significance for both basic neuroscience and potential drug development.

Following the isolation, characterization, and chemical synthesis of MII we initiated a study of its three-dimensional structure using 2D ^{1}H NMR spectroscopy and examined its structural stability in different solvent environments. By analogy with other α-conotoxins whose structures have been determined previously (*13*, *18*−*23*), it was anticipated that MII would contain elements of helicity. Furthermore, since the RP-HPLC retention time of MII increases upon oxidation of the reduced form, indicating an increase in the exposure of hydrophobic residues, it was of interest to examine the structure of MII in a variety of solution environments. With the expectation of a helical region in a relatively hydrophobic peptide, 30% TFE/H_2O was chosen. The structural data in this solvent are compared to those in aqueous solution and to a solvent with intermediate hydrophobic character, i.e., 30% CD_3CN/H_2O.

The high-resolution solution structure of MII reported here will be extremely valuable for interpreting structure−activity data and for the investigation and modeling of nAChR−ligand interactions. While our studies were in progress, a structure for MII in aqueous solution was reported (*24*). In the current paper we compare our NMR-based structural information for MII in three different solvent systems with that of Shon et al. (*24*) in aqueous solution as well as to other α-conotoxins that target neuronal nAChRs. In general, the structures are in good agreement, but it is clear that the presence of a hydrophobic solution environment enhances a helical region within MII and results in improved structural definition. As MII interacts with a membrane-bound receptor, it is interesting that there is increasing structural stabilization in hydrophobic environments.

EXPERIMENTAL PROCEDURES

Materials. Boc-L-amino acids and *p*-methylbenzhydrylamine (MBHA) resin were purchased from Novabiochem (San Diego, CA) and Peptide Institute (Osaka, Japan). Dichloromethane (DCM), *N*,*N*-diisopropylethylamine (DIEA), *N*,*N*-dimethylformamide (DMF), and trifluoroacetic acid (TFA), all peptide-synthesis grade, were obtained from Auspep (Melbourne, Australia). 2-(1*H*-Benzotriazol-1-yl)-1,1,3,3-tetramethyluronium hexafluorophosphate (HBTU) was purchased from Richelieu Biotechnologies (Quebec, Canada). Deuterated solvents were obtained from Cambridge Isotope Laboratories (Woburn, MA). All other chemicals were of analytical grade from commercial suppliers.

Peptide Synthesis. α-Conotoxin MII was chemically synthesized stepwise using *in situ* neutralization/HBTU activation protocols for Boc chemistry as previously described (*25*). The synthesis was performed on *p*-methylbenzhydrylamine (100−200 mesh) resin on an 0.2 mmol

scale. The following amino acid side chain protection was used: Asn(Xan), Cys(MeBzl), Glu(OcHxl), His(DNP), and Ser(Bzl). Each residue was coupled for 10 min, and coupling efficiencies were determined by the quantitative ninhydrin reaction (*26*). The average yield of chain assembly was 99.35%. Before HF cleavage the dinitrophenyl groups were removed by treatment with 20% β-mercaptoethanol, 10% DIEA, and 70% DMF for 2 h, prior to N-terminal Boc deprotection with 100% TFA. The resin was then washed with DCM and dried under nitrogen. The peptide was cleaved from the resin and simultaneously deprotected by treatment with 10 mL of HF/*p*-cresol/*p*-thiocresol [18:1:1 (v/v)] at 0 °C for 2 h. After evaporation of the HF, the crude product was precipitated and washed with cold diethyl ether (2 × 10 mL), dissolved in 20% acetonitrile (5 mL), and lyophilized after aqueous dilution. The crude material was oxidized in 146 mL of 0.1 M NH_4HCO_3 buffer (pH 8) at room temperature with vigorous stirring for 6 days and subsequently purified to homogeneity by preparative RP-HPLC (Vydac C_{18} column, 22 × 250 mm) using a linear gradient of 0−80% acetonitrile in water and 0.1% TFA over 80 min at a flow rate of 8 mL/min. Analytical RP-HPLC (Vydac C_{18} column, 4.6 × 250 mm) and ESMS (PE-Sciex API-III, Toronto, Canada) confirmed the purity and molecular weight of the synthetic peptide.

The disulfide connectivities of the synthetic peptide were confirmed by RP-HPLC coelution experiments with native material and by selective reductive alkylation (J.-P. Bingham, unpublished results; *27*). A mixture of synthetic and native material (2:1) was reduced with tris(2-carboxyethyl)phosphine (60 °C, 5 min) and the reaction terminated upon observation of discreet broadening of the monoisotopic distribution of the $[M + 2H]^{2+}$ ion. The resulting free thiols were alkylated with maleimide, and ESMS analysis demonstrated the presence of two alkyl groups. The corresponding material was purified by RP-HPLC and subjected to 17 cycles of Edman analysis. This identified the presence of the novel cysteine derivative cycles at positions 2 and 8 and unassigned cycles at positions 3 and 16, confirming that synthetic MII has the correct 2−8 (I−III) and 3−16 (II−IV) disulfide connectivities.

Circular Dichroism. Far-UV circular dichroism spectra were obtained on a Jasco J-300 spectropolarimeter calibrated with (+)-10-camphorsulfonic acid at 20 °C using a 0.01 cm path length. MII was dissolved in water (pH 4) at a concentration of 280 μM for all experiments. Each spectrum represents the average of 10 scans. Mean residue ellipticity $[\Theta]_{MR}$ is expressed in degrees square centimeter per decimole (deg·cm^2/dmol).

NMR Spectroscopy. Samples for ^{1}H NMR measurements contained 3 mM peptide in (a) 90% H_2O/10% D_2O or 99.99% D_2O at pH 3.9, (b) 30% d_3-TFE/H_2O, and (c) 30% CD_3CN/H_2O. All solvent percentages are by volume. Spectra were recorded at 15 and 25 °C on Bruker ARX-500 or DMX-750 spectrometers equipped with a shielded gradient unit. 2D NMR spectra were recorded in phase-sensitive mode using time-proportional phase incrementation for quadrature detection in the t_1 dimension (*28*). The 2D experiments included DQF-COSY (*29*), E-COSY (*30*), TOCSY (*31*) using a MLEV-17 spin lock sequence (*32*) with a mixing time of 80 ms, and NOESY (*33*) with mixing times of 50, 150, 250, and 350 ms. For DQF-COSY and E-COSY experiments, solvent suppression was achieved using selective low-power irradiation of the water resonance during a relaxation delay of 1.8 s. Solvent suppression for NOESY and TOCSY experiments was achieved using a modified WATERGATE sequence (*34*) in which two gradient pulses of 2 ms duration and 6 G cm^{-1} strength were applied on either side of a binomial 3-9-19 pulse. Spectra were routinely acquired over 6024 Hz (at 500 MHz) and 8012 Hz (at 750 MHz) with 4096 complex data points in F_2 and 400−600 increments in the F_1 dimension, with 16−64 scans per increment. Slowly exchanging NH protons were detected by acquiring a series of 1D and TOCSY spectra of the fully protonated peptide immediately following dissolution in 100% D_2O, 30% d_3-TFE/D_2O, or 30% CD_3CN/D_2O. $^3J_{H\alpha-H\beta}$ coupling constants were measured from E-COSY spectra, and $^3J_{NH-H\alpha}$ coupling constants were measured from DQF-COSY cross-peaks transformed to high digital resolution.

Spectra were processed on a Silicon Graphics Indigo workstation using XWIN-NMR (Bruker). The t_1 dimension was zero-filled to 2048 real data points, and 90° phase-shifted sine bell window functions were applied prior to Fourier transformation and baseline correction. Chemical shifts were referenced to internal DSS at 0.00 ppm. At 15 °C, the chemical shift of residual HDO in the solvent was H_2O, 4.92 ppm; CD_3CN, 4.72 ppm; and TFE, 4.92 ppm.

Structural Restraints. Distance restraints were derived primarily from the 350 ms NOESY spectrum recorded at 15 °C in 30% TFE/H_2O. Comparison was made to the 150 and 250 ms NOESY spectra to assess possible contributions from spin diffusion. Peak volumes were classified as strong, medium, weak, or very weak, corresponding to upper bound interproton distance restraints of 2.7, 3.5, 5.0, and 6.0 Å, respectively. Appropriate pseudoatom corrections were applied to nonstereospecifically assigned methylene and methyl protons (*35*). Backbone dihedral restraints were inferred from $^3J_{NH-H\alpha}$ coupling constants, with ϕ restrained to $-120 \pm 40°$ for a $^3J_{NH-H\alpha} \geq 8$ Hz and $-65 \pm 25°$ for $^3J_{NH-H\alpha} \leq 5$ Hz (*36*). Side chain χ_1 angles of residues Asn5, Glu11, and His12 were restrained to $-60 \pm 30°$ on the basis of the observed patterns of intraresidue NOEs and $^3J_{H\alpha-H\beta}$ coupling constants (*37*).

Structure Calculations. Three-dimensional structures were calculated using a simulated annealing and energy minimization protocol in the program X-PLOR 3.1 (*38*). In the first step an ab initio simulated annealing protocol (*39*) was used, starting from template structures with randomized ϕ and ψ angles and extended side chains, to generate a set of 20 structures. At this stage the disulfide bonds were included as pseudo-NOE restraints, and the simulated annealing protocol consisted of 20 ps of high-temperature molecular dynamics (1000 K) with a low weighting on the repel force constant and NOE restraints. This was followed for a further 10 ps with an increased force constant on the experimental NOE restraints. The disulfide bonds were then formally included, and the dihedral force constant was increased prior to cooling the system to 100 K and increasing the repel force constant over 15 ps of dynamics.

The NOE restraints were checked for violations, and ambiguous cross-peaks were resolved on the basis of interproton distances in the initial family of structures. A further 50 structures were calculated with the inclusion of ϕ and χ_1 dihedral angle restraints derived from spin−spin

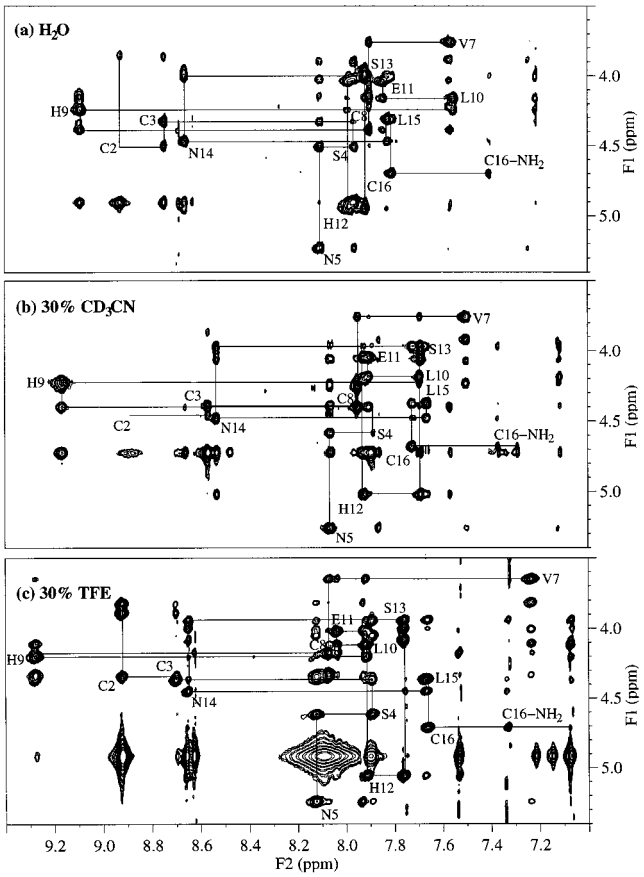

FIGURE 2: Fingerprint region of the 750 MHz NOESY spectrum of α-conotoxin MII at 15 °C in (a) 90% H_2O/10% D_2O, (b) 30% CD_3CN/H_2O, and (c) 30% d_3-TFE/H_2O showing the sequential $H\alpha-NH_{i+1}$ connectivities for residues 1−5 and 7−16. Residue assignments are indicated by the one-letter amino acid code and sequence number adjacent to the intraresidue NH−Hα NOE. Connections to the NH_2 protons of the amidated C-terminus are labeled C16−NH_2.

coupling constants. Refinement of these structures was achieved using the conjugate gradient Powell algorithm with 2000 cycles of energy minimization and a refined force field based on the program CHARMm (*40*). No hydrogen-bonding restraints were used, and all peptide bonds were defined as trans. Structures were analyzed using PROCHECK-NMR (*41*) and PROMOTIF (*42*) and were displayed using Insight II (version 95.0.3, MSI) and MOLMOL (*43*).

RESULTS

^{1}H Resonance Assignments. ^{1}H NMR spectra of α-conotoxin MII were recorded in three different solvents: H_2O, 30% CD_3CN/H_2O, and 30% d_3-TFE/H_2O. Sequence-specific resonance assignments were obtained using a well-established procedure (*44*) in which TOCSY and DQF-COSY spectra were used to identify amino acid spin systems and NOESY spectra were used to make sequential connections between these spin systems. Figure 2 shows the fingerprint region of the 750 MHz NOESY spectra of MII in H_2O, 30% CD_3CN/H_2O, and 30% TFE/H_2O and illustrates the sequential $H\alpha-NH_{i+1}$ connectivities. These connectivities are broken by the proline residue at position 6; however, strong $H\alpha-H\delta_{i+1}$ connectivities to this residue were observed in the NOESY spectrum recorded in D_2O to complete the sequential

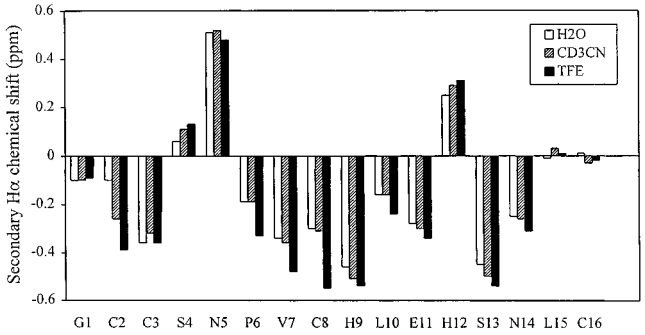

FIGURE 3: Secondary Hα chemical shifts, i.e., differences between observed chemical shifts and random coil shifts for the Hα resonances of α-conotoxin MII. As random coil Hα shifts have been shown to be insensitive to solvent (*56*), the random coil values used were for H_2O (*45*).

assignment. The presence of strong $H\alpha-H\delta_{i+1}$ NOEs and the absence of $H\alpha-H\alpha_{i+1}$ NOEs suggest that the Asn5−Pro6 peptide bond is in the trans conformation in all three solvent systems.

The backbone ^{1}H resonances of MII have good chemical shift dispersion in aqueous solution; however, the addition of 30% CD_3CN or 30% TFE resulted in an increased dispersion of both the NH and Hα resonances. This is readily apparent in Figure 2 where the amide chemical shift range increases from 1.6 ppm to more than 2.0 ppm in going from H_2O to 30% TFE/H_2O. This increase in chemical shift dispersion provides a first indication of an increase in structural definition with increased hydrophobic character of the solution environment of MII.

Secondary Structure. Secondary Hα chemical shifts, which represent the difference between the observed chemical shift and the random coil values of Wishart et al. (*45*), are given in Figure 3. In aqueous solution, an upfield trend (i.e., negative secondary shift) for the Hα resonances of residues 1−3, 6−11, and 13−14 suggests that MII consists predominantly of helical structural elements. On addition of CD_3CN or TFE this upfield trend is accentuated, particularly over residues 6−11. The effect of TFE in enhancing upfield shifts and, by implication, increasing the degree of helicity is significantly greater than that of CD_3CN. This is consistent with previous findings that TFE is conducive to helix stabilization in peptides with an inherent propensity to form helix (*46*, *47*). Not withstanding the observed differences between solvents, the *pattern* of secondary shifts across all the residues of MII is generally similar in each solvent, suggesting that the global fold is not perturbed by solvent.

Shon et al. (*24*) also reported significant upfield chemical shifts in aqueous solution and attributed this to helical conformations throughout the sequence with the exception of residues Asn5 and His12. The absolute values of the secondary shifts reported by Shon et al. (*24*) are significantly greater than reported here; however, this appears to be due to a referencing error in their work. Peaks were referenced to the water resonance at 4.76 ppm. At the temperature reported in their paper (275 K) the correct shift is closer to 5.02 ppm, thus making their apparent secondary shifts too large by a factor of ∼0.26 ppm. In our study, peaks were referenced to internal DSS and are thus unaffected by temperature dependence of the solvent resonance. The referencing error does not affect the conclusions of their

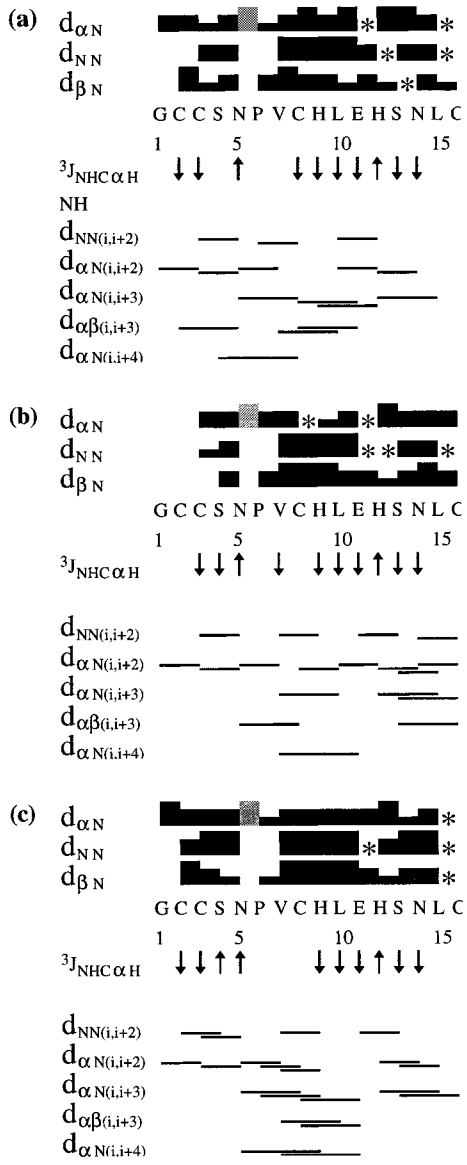

FIGURE 4: Summary of the sequential and medium-range NOEs and $^3J_{NH-H\alpha}$ coupling constants observed for MII in (a) 90% H_2O/10% D_2O, (b) 30% CD_3CN/H_2O, and (c) 30% TFE/H_2O. Filled bars indicate sequential connectivities observed in a 350 ms NOESY spectrum at 15 °C. Shaded bars correspond to sequential $H\alpha-H\delta_{i+1}$ connectivities for proline residues. The height of the bar indicates the strength of the NOE. Overlapping NOEs are indicated by an asterisk (*). ↑ indicate $^3J_{NH-H\alpha}$ coupling constants ≥8 Hz, and ↓ indicate $^3J_{NH-H\alpha}$ coupling constants ≤5 Hz.

paper but does overly emphasize the degree of helicity present in aqueous solution. From this study, it is clear that the peptide is helical over residues 6−11 in aqueous solution but that the helicity increases significantly upon addition of TFE.

The addition of acetonitrile or trifluoroethanol to the aqueous solution produced changes in a number of other spectral parameters, consistent with stabilization of the structure. Summaries of the sequential and medium-range NOEs and $^3J_{NH-H\alpha}$ coupling constants for MII in H_2O, 30% CD_3CN/H_2O, and 30% TFE/H_2O are shown in Figure 4. In H_2O, the observation of several strong $H\alpha-NH_{i+1}$ NOEs suggests a less than complete population of helical forms. In 30% CD_3CN or 30% TFE, the observation of generally weaker $H\alpha-NH_{i+1}$ and stronger $NH-NH_{i+1}$ connectivities,

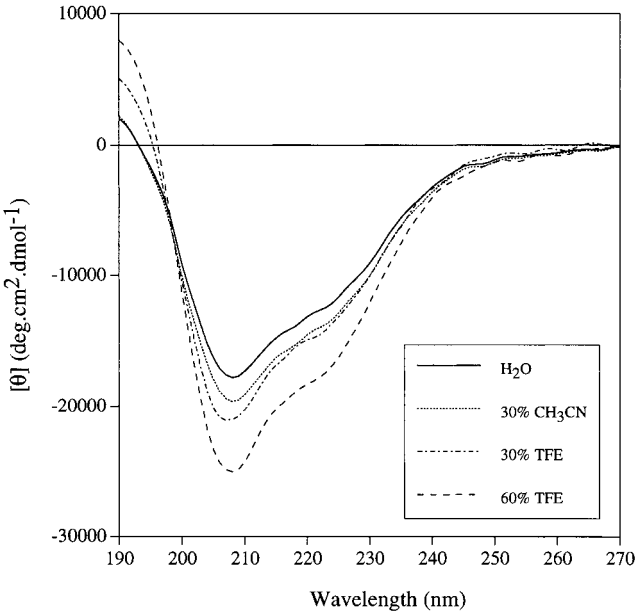

FIGURE 5: Far-UV circular dichroism spectra of α-conotoxin MII acquired with a peptide concentration of 280 μM at 25 °C, pH 4.

together with an increased number of $H\alpha-NH_{i+3}$ and $H\alpha-H\beta_{i+3}$ NOEs, suggests a stabilization of the structure which is predominantly α-helical in nature. This is supported by the coupling constant data, which show 7−8 residues having small $^3J_{NH-H\alpha}$ coupling constants (≤5 Hz) indicative of helical conformations. Residues 5 and 12 are the only ones to consistently have large $^3J_{NH-H\alpha}$ couplings in all three solvents. Both residues also exhibit $H\alpha-NH_{i+2}$ and lack $H\alpha-H\beta_{i+3}$ NOEs, and together with the coupling data this suggests the presence of turns near these residues. These flank the region of the molecule previously identified as having the greatest upfield shifts (6−11) and helical tendency.

To provide further support for the observed trend of increased structural stability in more hydrophobic solution environments, CD spectra of α-conotoxin MII were also recorded in a series of aqueous/organic solvent mixtures (Figure 5). These data confirm that the addition of 30% CH_3CN or 30% TFE induces a small increase in stability but does not induce any large conformational changes. The addition of higher concentrations of TFE further stabilized the structure (Figure 5).

Three-Dimensional Structure. It is evident that the secondary structure of α-conotoxin MII is similar in all the solvents studied but stabilized in the more hydrophobic environment provided by trifluoroethanol. For this reason we decided to calculate the three-dimensional structure of MII based on the data obtained in 30% TFE/H_2O. A set of 50 structures was calculated using 376 distance restraints derived from 150 intraresidual, 117 sequential, 89 medium-range, and 20 long-range NOEs and 12 dihedral angle restraints inferred from spin−spin coupling constants. All SA runs converged to produce structures with a common fold that were in excellent agreement with the experimental restraints and had low total energies. The 20 structures with the lowest energies were chosen to represent the solution structure of MII (Figure 6). In general, the structures exhibit no significant deviation from ideal covalent geometry, have good nonbonded contacts, and satisfy the experimental

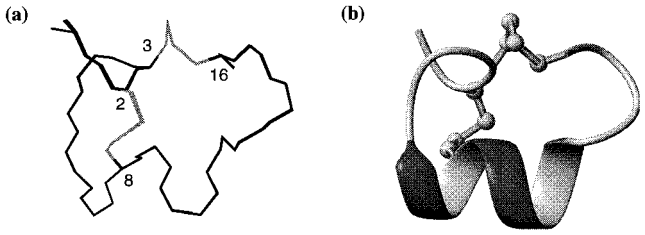

FIGURE 6: Three-dimensional solution structure of α-conotoxin MII. (a) Superimposition of the backbone heavy atoms of the 20 NMR-derived structures. The two disulfide bonds are shown in lighter shading, and the positions of the cysteine residues are labeled. (b) Schematic representation of the structure highlighting the location of the α-helix and disulfide bonds.

Table 1: Geometric and Energetic Statistics for the 20 Final Structures of α-Conotoxin MII[a]

rmsd from exptl restraints[b]	
interproton distances (Å) (376)	0.045 ± 0.001
dihedral angles (deg) (12)	1.01 ± 0.01
rmsd from idealized geometry	
bonds (Å)	0.012 ± 0.001
angles (deg)	3.04 ± 0.01
impropers (deg)	0.39 ± 0.01
energies (kcal mol^{-1})[c]	
E_{total}	32.5 ± 0.2
E_{NOE}	22.2 ± 0.2
E_{cdih}	0.74 ± 0.01
E_{L-J}	−59.1 ± 0.5
$E_{bond} + E_{angle} + E_{improper}$	61.3 ± 0.2
pairwise rmsd for backbone atoms (N, Cα, C) (Å)	
1−16	0.07 ± 0.06

[a] The values in the table are the mean ± standard deviation. [b] The number of restraints is shown in parentheses. None of the structures had distance violations >0.2 Å or dihedral angle violations >3°. [c] Force constants for the calculation of square-well potentials for the NOE and dihedral angle restraints were 50 kcal mol^{-1} Å^{-2} and 200 kcal mol^{-1} rad^{-2}, respectively. The Lennard-Jones van der Waals energy was calculated with the CHARMm empirical energy function.

restraints with minimal violations. The geometric and energetic statistics which define these 20 lowest energy structures are given in Table 1.

A superimposition of the family of structures in Figure 6 shows that, despite its rather small size, the polypeptide adopts a well-defined three-dimensional structure. In fact, the entire molecule, including side chains, is exceptionally well-defined with mean pairwise rms differences of only 0.07 ± 0.06 Å for the backbone heavy atoms and 0.34 ± 0.14 Å for all heavy atoms. The high precision is also indicated by high angular order parameters ($S \geq 0.99$) for all backbone ϕ and ψ angles and the majority of side chain χ_1 angles. Analysis of the family of 20 structures using PROCHECK-NMR (*41*) reveals that 84.6% of residues lie in the most favored regions of the Ramachandran plot with the remaining 15.4% in the additionally allowed regions.

Description of the Structure. The molecule folds into a highly compact globular structure consisting of a central region of α-helix and a series of overlapping β-turns at the N- and C-termini. The α-helix comprising residues 6−12 exhibits two turns and is amphipathic, with Cys8, His9, Glu11, and His12 on one side and Pro6, Val7, and Leu10 on the other. Remarkably, the hydrophobic residues of the α-helix are more exposed to the solvent than the charged/hydrophilic residues. However, this is consistent with the fact that MII is more hydrophobic when oxidized than when in the reduced form. At the N-terminus, residues 1−4 and 2−5 are involved in consecutive type I turns, and at the C-terminus residues 12−15 and 13−16 form type IV turns (*42*). The structures were analyzed to see if there was a well-defined pattern of either *i*, *i*+3 or *i*, *i*+4 hydrogen bonds that might further define the nature of the helix. Three *i*, *i*+4 hydrogen bonds between residues 6CO−10NH, 7CO−11NH, and 8CO−12NH were observed, indicating that regular α-helix rather than 3_{10}-helix is the dominant folded form. However, the fact that no amide protons persisted for more than 30 min following dissolution in D_2O suggests that all are relatively solvent exposed and that there is not likely to be strong hydrogen bonding within any region of the peptide.

The two disulfide bonds stabilizing the structure of MII have well-defined conformations across the family of calculated structures. The dihedral angle of the Cys2−Cys8 disulfide bond is representative of a left-handed spiral. The Cys3−Cys16 disulfide bond also has a χ_3 angle of −90°, but the combination of side chain dihedral angles does not fit any of the conformations commonly found for disulfides in protein structures (*48*).

Because MII is more hydrophobic in the oxidized form than in the reduced from by RP-HPLC, it was anticipated that many of the hydrophobic side chains may face outward. The derived three-dimensional structure shows this to be the case. A surface representation of MII illustrates a distinct hydrophobic face of the molecule (Figure 7). Interestingly, the molecular fold is such that this hydrophobic patch consisting of residues Pro6, Val7, and Leu10 is on the exposed face of the α-helix. Hydrophilic residues on the surface include Ser4, Asn5, and residues Glu11, His12, Ser13, and Asn14. The latter patch comprising residues with both polar and charged groups (Glu11−Asn14) may be responsible for initial recognition by the nAChR, with further stabilization of binding provided by the proximal hydrophobic residues. Analysis of the solvent accessibility of individual residues provides support for Pro6, Val7, Leu10, Glu11, and Asn 14 as potential residues for interaction with the nAChR as they are highly solvent exposed.

DISCUSSION

Effects of Solution Environment on the Conformation of α-Conotoxins. In studies of the conformations of biologically active peptides in solution there is frequent discussion as to what constitutes a biologically relevant solvent medium. When solubility considerations permit, aqueous solution is often the medium of choice; however, the intracellular environment contains a variety of other constituents including salts, membranes, and proteins. For peptides which interact with membrane receptors it may be that other media may better mimic biological sites of action. In any case, it is valuable to sample solution conformations in a range of different solvent environments so that any potential conformational transformations may be probed.

In this study, the structure of α-conotoxin MII in aqueous/organic solvent mixtures has been investigated using NMR spectroscopy to determine the susceptibility of the structure to conformational change. An examination of NMR data recorded in H_2O, 30% CD_3CN/H_2O, and 30% TFE/H_2O

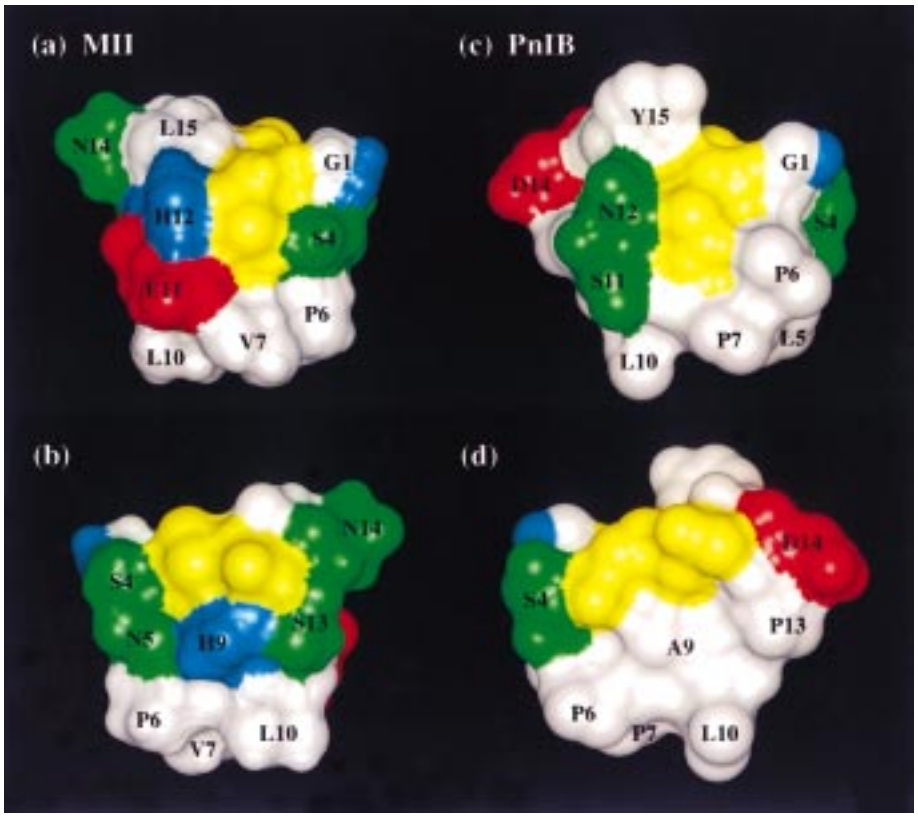

FIGURE 7: Comparison of the molecular surfaces of α-conotoxins MII (a and b) and PnIB (c and d). Views b and d are rotated by 180° about the vertical axis. The Connolly surfaces were calculated with a probe radius of 1.4 Å, and the residues are colored as follows: hydrophobic (white), cysteine (yellow), negatively charged (red), histidine and the N-terminus of Gly1 (blue), and uncharged hydrophilic (green). Visible residues are labeled with the one letter amino acid code and the sequence number.

allowed a comparison of the structural features in different solvent environments to be made. The similarity in the general trends in secondary Hα chemical shifts and other spectral parameters in the three solvents showed that there is no major conformational change with solvent, but there is a subtle increase in the degree of helicity with an increase in solvent hydrophobicity. It may be that this reflects more substantial "breathing" motions of the helix in aqueous solution so that the time-averaged degree of helicity decreases relative to the more hydrophobic solvents.

By contrast, the conformation of α-conotoxin GI, which possesses the smaller 3/5 spacing, remains relatively constant in the presence of up to 90% trifluoroethanol (*49*) and 50% acetonitrile (*13*). These results suggest that α-conotoxins with shorter inter-cysteine loops may be more conformationally constrained than α-conotoxins with the larger 4/7 spacing such as MII. This in turn reflects the fundamental difference in secondary structure and shape between the two main structural subclasses of α-conotoxins and highlights the importance of the spacing between disulfide bonds in determining the backbone conformation. The location and extent of regular secondary structure in α3/5-conotoxins is severely limited by the positioning of the disulfide bonds, and the major structural feature is a distorted 3_{10}-helix (residues 5−11) versus regular α-helix (residues 6−12) in α4/7-conotoxins (*20*, *22*).

It is of interest to note that MII adopts a single conformation in all the solvents studied. Many α-conotoxins studied to date have been reported to adopt more than one conformation in DMSO or aqueous solution (*18*, *23*), and this has been attributed to isomerization about the proline and/or tyrosine residue. Notably, PnIA and PnIB which have the same loop sizes as MII had multiple conformations in water; however, the addition of acetonitrile resulted in the stabilization of a single conformer (J. Gehrmann, personal communication). This appears to reflect the presence of only a single proline residue in MII, compared to three in PnIA and PnIB. The number of proline residues is therefore a crucial factor which should be considered in the design of analogue peptides for pharmacological studies.

Comparison with MII Determined in Aqueous Solution. While this study was in progress, the structure of MII determined in aqueous solution was reported by Shon et al. (*24*). The coordinates are not yet available from the Protein Data Bank; however, the data provided in their paper allow a preliminary comparison of the structures determined in H_2O and 30% TFE to be made. In general, the structures appear to be very similar, consisting of a central region of α-helix comprising residues 6−12 and overlapping β-turns or single turns of helix at the N- and C-termini. The terminal regions have been described as α-helix (Cys2−Ser4) and distorted 3_{10}-helix (Ser13−Cys16) in the structures calculated in aqueous solution (*24*). In our structures the N-terminus adopts overlapping type I β-turns consistent with the absence in 30% TFE of consecutive $H\alpha-NH_{i+3}$ and $H\alpha-H\beta_{i+3}$ NOEs characteristic of α-helix. These NOEs are also absent from the spectra acquired in H_2O; however, the differences between the structural elements described in the two studies probably only reflect differences in interpretation rather than significant structural changes.

$^3J_{NH-H\alpha}$ coupling constants are sensitive to local conformational changes, and hence a comparison of these data for

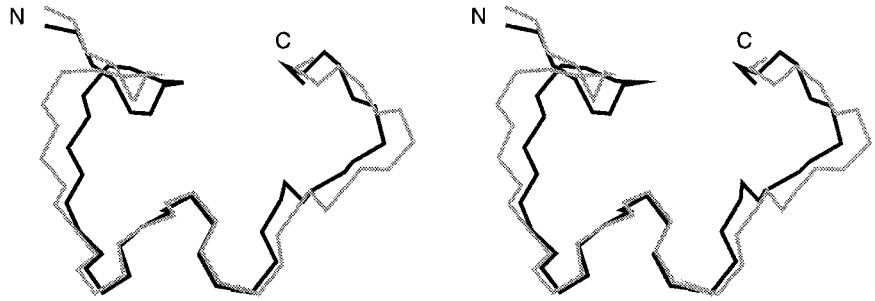

FIGURE 8: Stereoview of a superimposition of α-conotoxins MII (black) and PnIB (gray) over the backbone heavy atoms (N, Cα, C) of the entire molecule. The coordinates for PnIB were obtained from the Brookhaven Protein Data Bank (code 1AKG).

the two studies highlights any differences in conformations. Generally, the coupling constant data are in good agreement. The only exceptions are for Ser4, Leu15, and Cys16 where Shon et al. (*24*) reported couplings <5 Hz and our values are larger (7−8 Hz). The coupling constant for Ser4 is particularly interesting, as in CD_3CN we found it to be <5 Hz, but in TFE it is >8 Hz. The local conformation at this residue is clearly highly sensitive to the solution environment.

The structure of MII reported here is significantly better defined than the structure in water due to the inclusion of more than twice as many interresidue distance restraints, particularly medium- and long-range interactions. This appears to be a consequence of a larger number of NOEs from the use of TFE in the solvent medium and a high-field spectrometer (750 MHz). Consequently, both the precision and degree of convergence were higher. We chose 20 from 50 calculated structures to represent the structure of MII, although more than 90% of the total calculated structures converged to the same fold.

Comparison with Other α-Conotoxins and Implications for Receptor Binding. Recent high-resolution NMR and X-ray crystallography studies of the muscle-specific α-conotoxin GI (*13*, *20*) and the neuronal-specific α-conotoxins PnIA (*21*), PnIB (*22*), [Tyr^{15}]EpI (*50*), and MII (this study; *24*) provide a basis for understanding how these toxins differentially interact with subtypes of muscle and neuronal nAChRs. Hu et al. (*22*) have shown that the shape and surface charge distribution of the muscle-specific α-conotoxin GI differ dramatically from those of PnIA and PnIB which are specific for neuronal nAChRs. These variations in charge and molecular shape could be a means of selectively targeting the muscle or neuronal subtypes of nAChRs and also likely reflect structural differences at the various binding site interfaces. Understanding the structural basis of this specificity is a key step toward the rational design of subtype-selective agonists as therapeutic agents.

To identify structural and surface features that may be important for neuronal specificity, it is valuable to compare the structures of MII and PnIA/B. The NMR-derived structure of MII and the crystal structures of PnIA and PnIB (*21*, *22*) all incorporate the same global fold (Figure 8). Superimposition of the backbone heavy atoms of MII with PnIA and PnIB gives rms deviations of 0.95 and 0.94 Å, respectively. The X-ray crystal structures of PnIA and PnIB were determined from different crystal forms with different solvent contents, and the structure of MII was determined in solution; yet all are similar in three-dimensional structure. This shows that the α-conotoxin fold is generally stable and well-defined. The NMR method provides useful additional information in that it detects a subtle increase in structural stability as hydrophobicity increases.

Charge may be an important factor in determining specificity as the neuronal-specific α4/7-conotoxins are neutral, whereas the muscle-specific α-conotoxins typically have a net positive charge. Indeed, an arginine or lysine at either position 9 or 10 has been demonstrated to be critical for the activity of muscle-specific α-conotoxins GI, MI, and SI (*51*, *52*). However, positively charged residues are absent in the sequences of the neuronal-selective antagonists MII, PnIA, and PnIB. By contrast, the only charged residues in MII and PnIA/B are the negatively charged Glu11 and Asp14, respectively, and the positively charged N-terminus of Gly1 giving a net charge of zero. A comparison of the surfaces of MII and PnIB shows that the striking feature of both molecules is the large hydrophobic patch shown on the lower face of the molecules (Figure 7). Athough the positions of charged and other hydrophilic residues are quite different for MII and PnIB, a similar hypothesis to that proposed above for the binding of MII may also be applicable for PnIB. For example, Asp14 may be responsible for initial long-range electrostatic interactions with the nAChR and binding further stabilized by the proximal hydrophobic residues.

The recently discovered α-conotoxin EpI from *Conus episcopatus* displays striking sequence homology with the neuronal-specific α-conotoxins PnIA/B and ImI (Figure 1) and has been proposed to selectively inhibit α3β2 and/or α3β4 receptors (*12*). However, the primary structure of EpI differs considerably from MII, which is highly selective for the α3β2 subtype, suggesting that they may not target the same receptor type. Investigation of the binding selectivity of EpI, PnIA, and PnIB to a range of cloned nAChR subtypes expressed in *Xenopus* oocytes would provide important further insight into the interactions of α-conotoxins with neuronal nAChRs.

The X-ray crystal structure of [Tyr^{15}]EpI has also recently been determined and displays a backbone fold similar to that of the other α4/7-conotoxins (*50*). Hu et al. (*50*) have shown that the major difference between the surface charge distribution of [Tyr^{15}]EpI and PnIA/B reflects the differences in the first loop where Leu5 and Pro7 in PnIA/B are replaced by the two charged residues Asp5 and Arg7 in EpI. Interestingly, the first loop of EpI is identical to that of ImI, and the Asp5-Pro6-Arg7 triad has been demonstrated to be essential for the binding of ImI to the homomeric α7 receptor (*53*). Furthermore, the activities of EpI, which contains a sulfotyrosine at position 15, and its unsulfated analogue [Tyr^{15}]EpI were similar (*12*), suggesting that this site does

not interact with the receptor. These findings provide support for a role of the solvent-exposed residues of the α-helix (lower face of the molecules shown in Figure 7) in receptor binding, rather than the upper face of the molecules as previously suggested (*24*).

At present we can only speculate about the interaction of these toxins with neuronal nAChRs. However, given the recent findings of the importance of the α3β2 receptor type in the modulation of dopamine release and its relevance to the problems of addiction and psychosis, a structural understanding of the mode of interaction of α-conotoxin MII with the α3β2 interface is very important. The high-resolution structure of MII and comparison with other α-conotoxins reported here will facilitate the design of analogues to define the structural requirements for affinity and selectivity for subtypes of neuronal nAChRs and will provide direction for complementary mutagenesis on the nAChR to further identify the interacting residues (*54*, *55*). In addition, as side chain orientations are of paramount importance in defining pharmacophore models, the structure of MII is a potentially useful template for the design of selective small molecule inhibitors of neuronal nAChRs.

ACKNOWLEDGMENT

We thank Shu-Hong Hu and John Gehrmann for helpful discussions and Ian Brereton for assistance and maintenance of the 750 MHz spectrometer.

SUPPORTING INFORMATION AVAILABLE

Table S1 containing ^{1}H resonance assignments of α-conotoxin MII in H_2O, 30% CD_3CN/H_2O, and 30% TFE/H_2O and Figure S1 showing the angular order parameters (ϕ, ψ, and χ_1) for the 20 final structures (3 pages). Ordering information is given on any current masthead page.

REFERENCES

1. Myers, R. A., Cruz, L. J., Rivier, J. E., and Olivera, B. M. (1993) *Chem. Rev. 93*, 1923−1936.
2. Lewis, R., Alewood, P., Dooley, M., Martin, J., Drinkwater, R., Craik, D., and Andrews, P. (1996) *Today's Life Sci. 8*, 16−24.
3. Gray, W. R., Luque, A., Olivera, B. M., Barret, J., and Cruz, L. J. (1981) *J. Biol. Chem. 256*, 4734−4740.
4. McIntosh, M., Cruz, L. J., Hunkapiller, M. W., Gray, W. R., and Olivera, B. M. (1982) *Arch. Biochem. Biophys. 218*, 329−334.
5. Zafaralla, G. C., Ramilo, C., Gray, W. R., Karlstrom, R., Olivera, B. M., and Cruz, L. J. (1988) *Biochemistry 27*, 7102−7105.
6. Myers, R. A., Zafaralla, G. C., Gray, W. R., Abbott, J., Cruz, L. J., and Olivera, B. M. (1991) *Biochemistry 30*, 9370−9377.
7. Ramilo, C. A., Zafaralla, G. C., Nadasdi, L., Hammerland, L. G., Yoshikami, D., Gray, W. R., Kristipati, R., Ramachandran, J., Miljanich, G., Olivera, B. M., and Cruz, L. J. (1992) *Biochemistry 31*, 9919−9926.
8. McIntosh, J. M., Yoshikami, D., Mahe, E., Nielsen, D. B., Rivier, J. E., Gray, W. R., and Olivera, B. M. (1994) *J. Biol. Chem. 269*, 16733−16739.
9. Fainzilber, M., Hasson, A., Oren, R., Burlingame, A. L., Gordon, D., Spira, M. E., and Zlotkin, E. (1994) *Biochemistry 33*, 9523−9529.
10. Martinez, J. S., Olivera, B. M., Gray, W. R, Craig, A. G., Groebe, D. R., Abramson, S. N., and McIntosh, J. M. (1995) *Biochemistry 34*, 14519−14526.
11. Cartier, G. E., Yoshikami, D., Gray, W. R., Luo, S., Olivera, B. M., and McIntosh, J. M. (1996) *J. Biol. Chem. 271*, 7522−7528.
12. Loughnan, M., Bond, T., Atkins, A., Cuevas, J., Adams, D. J., Broxton, N. M., Livett, B. G., Down, J. G., Jones, A., Alewood, P. F., and Lewis, R. J. (1998) *J. Biol. Chem. 273*, 15667−15674.
13. Gehrmann, J., Alewood, P. F., and Craik, D. J. (1998) *J. Mol. Biol. 278*, 401−415.
14. Sargent, P. B. (1993) *Annu. Rev. Neurosci. 16*, 403−443.
15. Kulak, J. M., Nguyen, T. A., Olivera, B. M., and McIntosh, J. M. (1997) *J. Neurosci. 17*, 5263−5270.
16. Kaiser, S. A., Soliakov, L., Harvey, S. C., Luetje, C. W., and Wonnacott, S. (1998) *J. Neurochem. 70*, 1069−1076.
17. Picciotto, M. R., Zoli, M., Rimondini, R., Léna, C., Marublo, L. M., Pich, E. M., Fuxe, K., and Changeux, J.-P. (1998) *Nature 391*, 173−177.
18. Kobayashi, Y., Ohkubo, T., Kyogoko, Y., Nishiuchi, Y., Sakakibara, S., Braun, W., and Go, N. (1989) *Biochemistry 28*, 4853−4860.
19. Pardi, A., Galdes, A., Florance, J., and Maniconte, D. (1989) *Biochemistry 28*, 5494−5501.
20. Guddat, L. W., Martin, J. L., Shan, L., Edmundson, A. B., and Gray, W. R. (1996) *Biochemistry 35*, 11329−11335.
21. Hu, S.-H., Gehrmann, J., Guddat, L. W., Alewood, P. F., Craik, D. J., and Martin, J. L. (1996) *Structure 4*, 417−423.
22. Hu, S.-H., Gehrmann, J., Alewood, P. F., Craik, D. J., and Martin, J. L. (1997) *Biochemistry 36*, 11323−11330.
23. Gouda, H., Yamazaki, K., Hasegawa, J., Kobayashi, Y., Nishiuchi, Y., Sakakibara, S., and Hirono, S. (1997) *Biochim. Biophys. Acta 1343*, 327−334.
24. Shon, K.-J., Koerber, S. C., Rivier, J. E., Olivera, B. M., and McIntosh, J. M. (1997) *Biochemistry 36*, 15693−15700.
25. Schnölzer, M., Alewood, P., Jones, A., Alewood, D., and Kent, S. B. H. (1992) *Int. J. Pept. Protein Res. 40*, 180−193.
26. Sarin, V., Kent, S. B. H., Tam, J. P., and Merrifield, R. B. (1981) *Anal. Biochem. 117*, 147−157.
27. Jones, A., Bingham, J.-P., Gehrmann, J., Bond, T., Loughnan, M., Atkins, A., Lewis, R. J., and Alewood, P. F. (1996) *Rapid Commun. Mass Spectrom. 10*, 138−143.
28. Marion, D., and Wüthrich, K. (1983) *Biochem. Biophys. Res. Commun. 113*, 967−974.
29. Rance, M., Sørenson, O. W., Bodenhausen, G., Wagner, G., Ernst, R. R., and Wüthrich, K. (1983) *Biochem. Biophys. Res. Commun. 117*, 479−495.
30. Greisinger, C., Sørenson, O. W., and Ernst, R. R. (1987) *J. Magn. Reson. 75*, 474−492.
31. Braunschweiler, L., and Ernst, R. R. (1983) *J. Magn. Reson. 53*, 521−528.
32. Bax, A., and Davis, D. G. (1985) *J. Magn. Reson. 65*, 355−360.
33. Jeener, J., Meier, B. H., Bachmann, P., and Ernst, R. R. (1979) *J. Chem. Phys. 71*, 4546−4553.
34. Piotto, M., Saudek, V., and Sklenar, V. (1992) *J. Biomol. NMR 2*, 661−665.
35. Wüthrich, K., Billeter, M., and Braun, W. (1983) *J. Mol. Biol. 169*, 949−971.
36. Pardi, A., Billeter, M., and Wüthrich, K. (1984) *J. Mol. Biol. 180*, 741−751.
37. Wagner, G., Braun, W., Havel, T. F., Schaumann, T., Go, N., and Wüthrich, K. (1987) *J. Mol. Biol. 196*, 611−639.
38. Brünger, A. T. (1992) *X-PLOR Manual Version 3.1*, Yale University, New Haven, CT.
39. Nilges, M., Gronenborn, A. M., Brünger, A. T., and Clore, G. M. (1988) *Protein Eng. 2*, 27−38.
40. Brooks, B. R., Bruccoleri, R. E., Olafson, B. D., States, D. J., Swaminathan, S., and Karplus, M. (1983) *J. Comput. Chem. 4*, 187−217.
41. Laskowski, R. A., Rullmann, J. A. C., MacArthur, M. W., Kaptein, R., and Thornton, J. M. (1996) *J. Biomol. NMR 8*, 477−486.
42. Hutchinson, E. G., and Thornton, J. M. (1996) *Protein Sci. 5*, 212−220.

43. Koradi, R., Billeter, M., and Wüthrich, K. (1996) *J. Mol. Graphics 14*, 51−55.
44. Wüthrich, K. (1986) *NMR of Proteins and Nucleic Acids*, Wiley-Interscience, New York.
45. Wishart, D. S., Bigam, C. G., Holm, A., Hodges, R. S., and Sykes, B. D. (1995) *J. Biomol. NMR 5*, 67−81.
46. Dyson, H. J., Merutka, G., Waltho, J. P., Lerner, R. A., and Wright, P. E. (1992) *J. Mol. Biol. 226*, 795−817.
47. Sönnichsen, F. D., van Eyk, J. E., Hodges, R. S., and Sykes, B. D. (1992) *Biochemistry 31*, 8790−8798.
48. Richardson, J. S. (1981) *Adv. Protein Chem. 34*, 167−339.
49. Hider, R. C. (1985) *FEBS Lett. 184*, 181−184.
50. Hu, S.-H., Loughnan, M., Miller, R., Weeks, C. M., Blessing, R. H., Alewood, P. F., Lewis, R. J., and Martin, J. L. (1998) *Biochemistry 37*, 11425−11433.
51. Hann, R. M., Pagán, O. R., Gregory, L. M., Jácome, T., and Eterovic, V. A. (1997) *Biochemistry 36*, 9051−9056.
52. Groebe, D. R., Gray, W. R., and Abramson, S. N. (1997) *Biochemistry 36*, 6469−6474.
53. Quiram, P. A., and Sine, S. M. (1998) *J. Biol. Chem. 273*, 11007−11011.
54. Quiram, P. A., and Sine, S. M. (1998) *J. Biol. Chem. 273*, 11001−11006.
55. Harvey, S. C., McIntosh, J. M., Cartier, G. E., Maddox, F. N., and Luetje, C. W. (1997) *Mol. Pharmacol. 51*, 336−342.
56. Merutka, G., Dyson, H. J., and Wright, P. E. (1995) *J. Biomol. NMR 5*, 14−24.

BI981535W